

# Enhancement of naphthalene hydrogenation over PtPd/SiO<sub>2</sub>–Al<sub>2</sub>O<sub>3</sub> catalyst modified by gold

B. Pawelec<sup>a,\*</sup>, V. La Parola<sup>a</sup>, S. Thomas<sup>b</sup>, J.L.G. Fierro<sup>a</sup>

<sup>a</sup> *Institute of Catalysis and Petrochemistry, CSIC, c/Marie Curie, 2, Cantoblanco, 28049 Madrid, Spain*

<sup>b</sup> *Fraunhofer Institute for Factory Operation and Automation IFF Magdeburg,*

*Department of Process and Plant Engineering, Sandtorstrasse 22, 39106 Magdeburg, Germany*

Received 12 January 2006; received in revised form 28 February 2006; accepted 1 March 2006

Available online 18 April 2006

## Abstract

This contribution describes the effect of support (amorphous silica–alumina: ASA and multi-wall carbon nanotubes: MWNT) on the catalytic response of bimetallic PtPd catalysts in naphthalene hydrogenation (HYD). In addition, the effect of Au incorporation on the activity of PtPd/ASA catalyst was studied. The ternary AuPtPd/ASA catalyst was prepared by the simultaneous reduction of metal precursors by ethanol in the presence of poly(*N*-vinyl-2-pyrrolidone) (PVP), whereas binary PtPd/ASA and PtPd/MWNT catalysts were prepared by a conventional impregnation method. The catalysts were characterized using chemical analysis, nitrogen adsorption–desorption isotherms at 77 K, CO chemisorption, FTIR spectra of chemisorbed CO, transmission electron microscopy (TEM), DRIFT of adsorbed NH<sub>3</sub>, X-ray diffraction (XRD), X-ray photoelectron spectroscopy (XPS) and thermogravimetric analysis (TGA) measurements. Under the reaction conditions employed ( $T = 448\text{--}463\text{--}483\text{ K}$ ,  $P = 2.0\text{ MPa}$ ,  $\text{WHSV} = 45.7\text{ h}^{-1}$ ), the ternary AuPtPd/ASA catalyst showed highest naphthalene conversion and lowest deactivation among the catalysts studied. The S-tolerance of this catalyst was confirmed during simultaneous naphthalene and toluene HYD in the presence of dibenzothiophene (DBT; 100 ppm of S). The enhanced activity and S-tolerance observed with the AuPtPd/ASA catalyst was related to its larger metal surface exposure, as determined by XPS, and the “ensemble” effect of the Au<sub>70</sub>Pd<sub>30</sub> and Au<sub>42</sub>Pd<sub>58</sub> alloy particles formed on ASA, as demonstrated by XRD. It is proposed that surface gold weakens the adsorption of aromatic compounds (toluene/naphthalene/DBT), facilitating product desorption. Contrary to acidic AuPtPd/ASA, the less acidic PtPd/MWNT catalyst did not show S-resistance in reaction of benzene HYD in the presence of 1-butanethiol. The contribution of the acid sites of support to catalyst S-resistance and their deactivation by coke are discussed.

© 2006 Elsevier B.V. All rights reserved.

**Keywords:** Gold; Platinum; Palladium; Naphthalene hydrogenation; Multi-walled carbon nanotubes; Silica–alumina

## 1. Introduction

To comply with new diesel environmental requirements the density of middle distillate fuels needs to be lower than 845 kg m<sup>-3</sup> whereas cetane number higher than 51 [1]. This could be achieved by saturation of the polyaromatics [2], e.g., the total saturation of naphthalene to decalin reduces the fuel density to ca. 900 kg m<sup>-3</sup> and improves cetane number up 38. Since both parameters are still below the new diesel specifications, the ring opening of naphthenic structures is practiced with the aim to upgrading heavy petroleum fractions [2]. Thus,

it was recently shown that under industrially employed conditions the selective ring opening of naphthenic structures could be successfully performed using a Pt–Ir-based catalyst [3,4].

The use of noble metal catalysts, which are highly active for the hydrogenation (HYD) reactions, opens possibility of preparing alternatives to conventional CoMo catalysts which allow only a moderate saturation of the polyaromatics due to the thermodynamic constraints of the aromatic saturation at high temperature [5–7]. The high activity of Pt- and Pd-based catalysts in hydrogenation reactions is due to the high ability of Pt and Pd to dissociate hydrogen, which allows work to be carried out at temperatures lower than in the case of CoMo catalysts. In general, the bimetallic PtPd catalysts are more active than the monometallic Pt and Pd counterparts [7] being the Pd/Pt atomic ratio equal to 0.4 the most effective for hydrogenation and hydrogenolysis/ring-opening reactions [8,9]. Contrary to Pt

\* Corresponding author. Fax: +34 915854760.

E-mail address: [bgarcia@icp.csic.es](mailto:bgarcia@icp.csic.es) (B. Pawelec).

URL: <http://www.icp.csic.es/eac/index.htm> (B. Pawelec).

and Pd, the use of gold for reactions involving hydrogen has been investigated only recently [10,11 and references within]. The reason is that gold, with a completely filled Au d-band, has a limited capacity to dissociate H<sub>2</sub> molecules [11] and probably because of the very low activity of gold catalysts having too large metal particles [12]. This situation is drastically changed when the gold particles are very small [11]. Thus, the gold-based catalysts were found to be active in partial and selective hydrogenation reactions [10–12].

Unfortunately, the Pt and Pd catalysts are easily poisoned even by few ppm of sulfur limiting their use to two-stage catalytic process involving initially hydrodesulphurization (HDS) and hydrodenitrogenation (HDN) followed by hydrodearomatization (HDA) and selective ring opening to improve the cetane number [3–6]. Thus, the challenge is to tailor Pt or Pd catalyst possessing a high tolerance to S-poisoning. According to recent studies on gold catalysts, the possible solution is the addition of Au to Pt- or Pd-catalysts [13–19]. This is because of the importance of geometric effects on catalysis by Pt(Pd) [13] and the well known affinity of gold for S-compounds [11]. This strong affinity of gold for sulfur compounds is exploited in gas sensors for the detection of H<sub>2</sub>S [11], and it was confirmed for monometallic Au and binary AuPt(Pd) catalysts tested in different reactions involving S-compounds [14–19]. The enhancement of the hydrogenation activity and the S-tolerance of binary AuPd/SiO<sub>2</sub>–Al<sub>2</sub>O<sub>3</sub> catalysts tested in the simultaneous hydrogenation of naphthalene and toluene in the presence of dibenzothiophene (DBT) was related to modifications of the electronic properties of the metal atom upon interaction with the acid sites and upon intermetallic interaction [14]. However, to our knowledge, the study on the hydrogenation activity and thio-tolerance of ternary AuPtPd formulation has not been yet reported in the literature.

Early studies on catalyst thio-resistance demonstrated that its sulfur tolerance could be enhanced modifying the physicochemical characteristics of the metal atoms by: (i) adding a transition metal promoter; (ii) alloying (for example, PtPd alloy); (iii) a decrease in the metal particle size; or (iv) using acidic supports such as zeolites [5,6]. In the latter case, it is believed that the high S-tolerance of zeolite-based Pt- or Pd-catalysts arises from the electron-deficient Pt<sup>δ+</sup> or Pd<sup>δ+</sup> particles formed upon interaction of the small metal particles with the Brønsted acid sites of the zeolite, which in turn lowers the strength of the sulfur–metal (S–M) bond [20,21]. On the contrary, the intrinsic thio-resistance of the Pt/Pd pair was postulated using non-acidic Mg/Al mixed oxide [22] suggesting that the contribution of the acid sites of the support to catalyst thio-resistance is of less importance than is commonly believed. Thus, the real factors governing the sulfur resistance of metallic catalysts remain still unclear and it is more likely that an optimum needs to be found between the following conjugated effects: aromatics and sulfur adsorption, metallic phase properties (such as structure, surface composition and electronic modification) as well as the properties of support [23].

Recently, the strategy in catalyst tailoring involves the substitution of the acid supports such as alumina by less acidic carriers such as silica–alumina [7,14,17] or even by basic sup-

ports such as Mg/Al basic mixed oxides [22]. This is because the acid sites of support favor cracking reactions to low molecular weight compounds that are outside of the diesel range (mainly gases) as well as enhanced catalyst deactivation by coking. Besides the controlled surface acidity, the support needs to have adjustable mesoporosity in order to allow the diffusion of voluminous molecules inside the pores [24]. Among the possible less acidic carriers, one-dimensional multi-walled carbon nanotubes (MWNT) are interesting candidates because of their large meso- and macroporous structure [25]. Carbon nanotubes (CNT) and fibers as supports have been already applied for reactions involving hydrogen [26–33]. Indeed, our recent study on PtPd/MWNT catalyst tested in simultaneous toluene and naphthalene HYD in the presence of DBT demonstrated its exceptionally high initial intrinsic hydrogenation activity [33]. In comparison with one-dimensional MWNT, the ASA support offers larger BET specific areas, acidity and different porous structure.

In keeping with the foregoing, this paper extends our previous investigation on the use of MWNT [33] and amorphous ASA [7,14,17] as supports and Au as promoter of Pt- and Pd-based catalysts [14–18] with the aim to investigate the hydrogenation behavior of ternary AuPtPd formulation in comparison with binary PtPd systems. The hydrogenation activities of catalysts were compared in naphthalene hydrogenation whereas thio-resistance of ternary sample was confirmed during simultaneous naphthalene and toluene hydrogenation in the presence of dibenzothiophene (DBT; 100 ppm of S). The S-poisoning of PtPd/MWNT catalyst was confirmed in benzene hydrogenation in the presence of 1-butanethiol. Careful investigation of the catalyst structure was accomplished using several techniques – chemical analysis, N<sub>2</sub> adsorption–desorption isotherms, XRD, FTIR of adsorbed CO, CO chemisorption, TEM, TPD-MS, DRIFT spectra of adsorbed NH<sub>3</sub>, TGA and XPS measurements – in an attempt to establish a relationship between activity and catalyst structure.

## 2. Experimental

### 2.1. Catalyst preparation

#### 2.1.1. Supports employed

A commercially available amorphous SiO<sub>2</sub>–Al<sub>2</sub>O<sub>3</sub> support containing 28 wt.% alumina (SMR 5-473; Si/Al=0.62 atomic ratio; BET=394 m<sup>2</sup> g<sup>-1</sup>; average pore diameter 7.5 nm; pore volume 118 cm<sup>3</sup> g<sup>-1</sup>), kindly supplied by Grace Davison Chemical, was calcined in air at 773 K for 3 h prior to catalyst preparation.

The multi-wall carbon nanotube (hereafter MWNT; BET=126 m<sup>2</sup> g<sup>-1</sup>; average pore diameter=9.2 nm; pore volume=40.7 cm<sup>3</sup> g<sup>-1</sup>) support was supplied by Sun Nanotech Co. Ltd. According to the specifications of the manufacturer, the carbon nanotubes are 10–30 nm in diameter and 1–10 μm in length, and their composition is as follows: multi-wall carbon nanotubes >80%; amorphous carbon <10; 1.21% of Fe<sub>2</sub>O<sub>3</sub>; 1.04% of NiO; 2.02% of Al<sub>2</sub>O<sub>3</sub>; 1.76% of SiO<sub>2</sub>; 3.97% of other elements. Before catalyst preparation, the MWNT was treated with HNO<sub>3</sub> (concentration 65%) at 383 K for 12 h

in order to introduce –OH groups onto carrier, which are necessary to anchor the metal precursors on the surface. In a previous work [33], it was shown HNO<sub>3</sub>-functionalization of MWNT develops strong acidic groups (carboxylic anhydride, carboxylic, lactone) and also increases the population of less acidic groups (anhydride, phenol, ether, carbonyl, quinone) by a factor of about 4.

### 2.1.2. Ternary sample

The AuPtPd/ASA catalyst was obtained by alcohol reduction of the metal precursors and stabilization of the metal clusters with the polymer poly(*N*-vinyl-2-pyrrolidone) (PVP) [34]. The procedure followed has been described elsewhere [15,16]. In short, the appropriate quantities of PtCl<sub>2</sub>, PdCl<sub>2</sub> and HAuCl<sub>4</sub> (all reagents were from Aldrich Co.) were dissolved in 400 ml of an ethanol/water (1/1, v/v) solution containing the PVP (MW = 10,000). The weight ratio of the PVP over the metal precursor was about 5. After adding the support to the solution, the suspension was stirred and refluxed at 363 K for 5 h under nitrogen. The excess of liquid was removed in a rotary evaporator and the solid was washed several times to eliminate the free PVP and the chloride ions. Finally the samples were dried in an oven at 343 K and then calcined in air at 673 K for 1 h. At this temperature PVP decomposes completely.

### 2.1.3. Binary catalysts

The PtPd/ASA catalyst was prepared by simultaneous wet impregnation of the ASA carrier with an aqueous solution (pH 7) of the metal nitrates: Pt(NH<sub>3</sub>)<sub>4</sub>(NO<sub>3</sub>)<sub>2</sub> (Aldrich, purity 99%) and Pd(NO<sub>3</sub>)<sub>2</sub>·6H<sub>2</sub>O (Fluka, purity 98%). Once adsorption equilibrium had been reached, excess water was removed in a rotary evaporator until dryness. Then, the impregnates were dried at 383 K in air for 12 h and calcined in air at 773 K for 2 h.

The PtPd/MWNT catalyst was prepared by simultaneous wet impregnation of the functionalized MWNT carrier with an aqueous solution (pH=0) of the metal precursors H<sub>2</sub>PtCl<sub>6</sub> (Alfa Aesar) and H<sub>2</sub>PdCl<sub>4</sub>, the latter prepared from PdCl<sub>2</sub> (Fluka) and a stoichiometric quantity of 10% HCl (with moderate heating of the mixture and final adjustment of the required volume with water). After adsorption equilibrium had been reached, the excess water was removed until dryness in a rotary evaporator. Catalyst drying was performed in air at 333 K overnight, followed by decomposition of the salts under He at 673 K for 2 h.

Table 1  
Physicochemical characteristics of the calcined catalysts

Catalyst	Metal loading <sup>a</sup> (wt.%)			BET <sup>b</sup> (m <sup>2</sup> g <sup>-1</sup> )	Pore size <sup>b</sup> (nm)	XRD <sup>c</sup> phase (%)
	Pt	Pd	Au			
AuPtPd/ASA	0.68	0.65	0.30	430	5.5	PdO/PtO; Au <sup>0</sup> (15), Au <sub>70</sub> Pd <sub>30</sub> (28), Au <sub>42</sub> Pd <sub>58</sub> (57)
PtPd/ASA	0.72	0.74	–	387	7.2	PdO/PtO, Pt <sup>0</sup>
PtPd/MWNT	0.75	0.72	–	140	9.1	Pt <sub>48</sub> Pd <sub>52</sub> (65), Pd <sup>0</sup> (35)

<sup>a</sup> As determined by chemical analysis.

<sup>b</sup> Specific BET area and average pore diameter as determined from N<sub>2</sub> adsorption–desorption isotherms at 77 K.

<sup>c</sup> Crystal phases as determined by XRD. Peak percentages are given in parentheses.

## 2.2. Characterization of the catalysts

### 2.2.1. Chemical analysis

The metal loadings of the calcined catalysts were determined using a Perkin-Elmer Optima 3300DV inductively coupled plasma atomic absorption spectrometer. The chemical compositions of the oxide catalysts are summarized in Table 1.

### 2.2.2. N<sub>2</sub> adsorption–desorption isotherms

The textural properties of the calcined catalysts were measured by adsorption–desorption of nitrogen at 77 K with a Micromeritics TriStar 3000 apparatus. The specific surface areas of the samples were determined from the nitrogen adsorption data using the BET method in the 0.005–0.25 *P/P*<sup>0</sup> range. Pore distributions were calculated from the desorption branch of the corresponding nitrogen isotherm employing the BJH method.

### 2.2.3. X-ray diffraction (XRD)

The powder X-ray diffraction measurements for the structure determination were carried out according to the step-scanning procedure (step size 0.02°; 0.5 s) with a computerized Seifert 3000 diffractometer using Ni-filtered Cu Kα (λ = 0.15406 nm) radiation and a PW 2200 Bragg-Brentano θ/2θ goniometer equipped with a bent graphite monochromator and an automatic slit. The assignment of the various crystalline phases was based on the JPDS powder diffraction file cards. Metal particle sizes were calculated from the line broadening of the most intense peak using the Scherrer equation [35]. The molar composition of Pt<sub>x</sub>Pd<sub>y</sub> and Au<sub>x</sub>Pd<sub>y</sub> alloys were obtained from the lattice parameter shifts, calculated from the angular position of the metal reflections according to the Vegard's law [36]. The precision of these calculated values was determined mainly from the error on the lattice parameters and was estimated to be about 5%.

### 2.2.4. Low- and high-resolution transmission electron microscopy (HRTEM)

For low and high magnification TEM study, the reduced (H<sub>2</sub>, 573 K) catalysts were crushed and ultrasonically dispersed in acetone at room temperature and then spread on a holey carbon-copper microgrid. TEM images were collected on a Joel TEM-3000F microscope operating at 300 kV.

### 2.2.5. CO chemisorption

Volumetric CO chemisorption isotherms at 303 K were obtained in order to estimate the amount of chemisorbed CO on

the samples reduced under H<sub>2</sub> at 573 K for 1 h and then outgassed at 10<sup>-5</sup> mbar. After cooling the samples to room temperature, CO was admitted and the first isotherm was measured. Extrapolation of the linear part of the isotherm to zero pressure provided the amount of strongly chemisorbed CO.

### 2.2.6. FTIR-CO

The infrared spectra of chemisorbed CO were recorded with a Nicolet 5ZDX Fourier transform spectrophotometer, working with a resolution of 4 cm<sup>-1</sup> over the entire spectral range and averaged over 100 scans. The samples, in the form of self-supporting wafers (thickness ca. 10 mg cm<sup>-2</sup>), were reduced in flowing hydrogen at 573 K for 1 h, and then outgassed under a vacuum at the same temperature for 1 h. After admission of CO at room temperature (30 mbar), the fraction of physically adsorbed molecules was removed by outgassing at room temperature for 15 min. Net infrared spectra of chemisorbed CO were obtained after subtraction of the background spectrum of the solid.

### 2.2.7. DRIFTS spectra of adsorbed NH<sub>3</sub>

The in situ DRIFT spectra of adsorbed NH<sub>3</sub> were recorded with a Nicolet 5ZDX FT spectrophotometer equipped with a Harrick diffuse reflectance accessory (HVC-DRP cell). The procedure followed during both measurements has been described elsewhere [37]. The samples were pre-reduced at 573 K for 0.5 h. After reduction, the samples were cooled under a flow of He and then treated with NH<sub>3</sub> (5% NH<sub>3</sub>-He) at room temperature and ambient pressure by passing NH<sub>3</sub>/He through the cell for 30 min. The semiquantitative comparison of catalyst acidity was accomplished using Gaussian deconvolution.

### 2.2.8. X-ray photoelectron spectroscopy (XPS)

Photoelectron spectra of used catalysts were recorded on a VG Escalab 200R electron spectrometer equipped with a hemispherical electron analyzer, using an Mg K $\alpha$  ( $h\nu = 1253.6$  eV) X-ray source. The samples, kept under octane to avoid contact with air, were placed in the pretreatment chamber and degassed at 10<sup>-6</sup> mbar. Then they were transferred to the ion-pumped analysis chamber, in which residual pressure was kept below  $4 \times 10^{-9}$  mbar during data acquisition. The binding energy (BE) of the C 1s peak at 284.9 eV was taken as an internal standard. The accuracy of the BE values was  $\pm 0.1$  eV. The peaks were fitted by a non-linear least squares fitting program using a properly weighted sum of Lorentzian and Gaussian component

curves after background subtraction according to Shirley [38] and Sherwood [39]. Surface atomic concentration was evaluated from peak areas using appropriate sensitivity factors built in the VG instrument software.

### 2.2.9. Thermogravimetric analysis (TGA)

The amount of coke deposited on the catalysts was determined with thermogravimetric TGA/SDTA851<sup>e</sup> equipment (Mettler Toledo), measuring the weight change in the coked catalysts during oxidation. The burning of coke was carried out by raising sample temperature to a final temperature of 1073 K at a rate of 10 K min<sup>-1</sup> in a 20% O<sub>2</sub>/N<sub>2</sub> mixture.

### 2.2.10. Hydrogenation of naphthalene

The hydrogenation (HYD) of naphthalene was performed in a continuous-down-flow fixed bed stainless steel reactor (9.5 mm ID and 130 mm length). Details have been given elsewhere [33]. The molar flow rate of the model feed (naphthalene dissolved in hexadecane) was 2.2 mmol h<sup>-1</sup>. Activity tests were performed using 0.25 g of powder catalyst diluted with SiC (0.25 mm) at a volume ratio of 1:5. Before activity tests the samples were isothermally reduced at 573 K for 3.5 h with 1:5 vol. H<sub>2</sub>/N<sub>2</sub> mixtures (a flow rate 90 mL min<sup>-1</sup>; atmospheric pressure; heating rate of 4 K min<sup>-1</sup>). The activities of catalysts were measured at  $T = 448, 463$  and 483 K, 2.0 MPa of total pressure, a weight hourly space velocity (WHSV) of 45.7 h<sup>-1</sup> and an H<sub>2</sub>/feed ratio of 220 L(N) L<sup>-1</sup>. Product liquids were condensed after depressurization at the reactor outlet, typically accumulated for 1 h. Liquid samples were analyzed by GC with FID (Varian chromatograph Model Star 3400 CX) equipped with a 30 m  $\times$  0.53 mm DB-1 column (J&W Scientific). Besides the relatively high conversion observed for all catalysts, the reaction was free of mass transport effects since, according to the Weisz-Prater parameter ( $\Phi$ ), conversion was always proportional to the mass of the catalyst or to the inverse of flow [40].

For naphthalene HYD, the initial turnover frequency (TOF; s<sup>-1</sup>) was calculated from reaction rates and the number of exposed surface metal atoms derived from the CO chemisorption data and compared with that derived from the metal particle size determined from TEM analysis (Table 2), whereas activity under steady-state conditions was described in terms of the quasi-turnover frequency number (QTOF; s<sup>-1</sup>), using a specific reaction rate according to Eq. (1):

$$r = \frac{XF}{m} \quad (1)$$

Table 2  
Physicochemical characterization of the catalysts after reduction at 573 K

Catalyst	CO uptake <sup>a</sup> ( $\mu\text{mol CO}_{\text{cat}}^{-1}$ )	Particle size <sup>b</sup> (nm)	B <sub>1450</sub> <sup>c</sup> (au)	B <sub>1450</sub> /L <sub>1300</sub> <sup>c</sup> ratio
AuPtPd/ASA	5.0	22.0	1.9	0.5
PtPd/ASA	15.7	27.9	2.9	0.6
PtPd/MWNT	11.0	7.8	0.4	0.1

<sup>a</sup> CO uptake as determined from CO chemisorption.

<sup>b</sup> Main metal particle size as determined by TEM measurements of the reduced samples.

<sup>c</sup> Brønsted acidity and Brønsted-to-Lewis (B<sub>1450</sub>/L<sub>1300</sub>) acidity ratio as determined by DRIFTS of adsorbed NH<sub>3</sub> from area of the bands at 1450 and 1300 cm<sup>-1</sup>, respectively.

where  $r$  is the specific rate ( $\mu\text{mol mol}_{\text{Me}}^{-1} \text{s}^{-1}$ ),  $X$  the conversion of naphthalene,  $F$  the molar flow rate of naphthalene ( $\mu\text{mol s}^{-1}$ ), and  $m$  refers to the metal loading per gram of catalyst ( $\text{mol g}_{\text{cat}}^{-1}$ ). Catalyst deactivation was calculated from the equation  $[(X_{1h} - X_{5h})/X_{1h} \times 100\%]$ . Apparent activation energies were calculated from Arrhenius plots obtained from the pseudo-first-order reaction constant  $k$  ( $\text{mmol g}_{\text{cat}}^{-1} \text{h}^{-1}$ ), calculated from steady-state conversions of naphthalene at three different temperatures (448, 463 and 483 K) according to Eq. (2):

$$k = - \left( \frac{F}{m_{\text{cat}}} \right) \ln(1 - X) \quad (2)$$

### 2.2.11. Study on the catalyst thio-resistance

In order to investigate the S-poisoning of the PtPd/MWNT catalyst, this sample was tested in a reaction of benzene HYD in the presence of 1-butanethiol (5 ppm of S) in the same reactor described above. Hexane was employed as solvent. The reaction conditions were:  $T=408$  K, 2.0 MPa of total pressure, WHSV of  $39.6 \text{ h}^{-1}$  and  $\text{H}_2/\text{feed}$  ratio of  $220 \text{ L(N) L}^{-1}$ . Besides unreacted benzene and 1-butanethiol, only cyclohexane was detected. The thio-resistance of the AuPtPd/ASA catalyst was verified in simultaneous naphthalene and toluene HYD in the presence of DBT. The reaction was carried out in the same apparatus described above. The reaction conditions were:  $T=523\text{--}548\text{--}573$  K, 2.0 MPa of total pressure, WHSV of  $41.2 \text{ h}^{-1}$  and a  $\text{H}_2/\text{feed}$  ratio of  $202 \text{ L(N) L}^{-1}$ . Besides unreacted DBT, naphthalene and toluene, the only products detected were biphenyl (BP), cyclohexylbenzene (CHB), tetralin, decalin and methylcyclohexane (MCH). For this catalyst, the activity is described in terms of toluene, naphthalene and DBT conversions.

## 3. Results and discussion

### 3.1. Characterization of the catalysts

Physicochemical characteristics of ASA- and MWNT-supported catalysts are shown in Table 1. The chemical analysis of the bimetallic catalysts revealed similar Pt and Pd content (ca. 0.7 wt.% of each), but the Au content in the ternary system was lower (0.30 wt.% Au). The final metal loadings of calcined catalysts was somewhat lower than the nominal one (Au: 0.5 wt.%; Pt and Pd: 1.0 wt.%).

The textural properties of the oxide catalysts were determined by means of nitrogen adsorption–desorption isotherms at 77 K (not shown here). According to the IUPAC classification, the nitrogen adsorption–desorption isotherms of the ASA-supported catalysts are of Type IVa with hysteresis loop between a Type H1 and H2 [4,41]. The former type of hysteresis loop is typical for materials having a narrow distribution of uniform pores whereas the latter is associated with materials having complex interconnected networks of pores with different shape and size. Thus, the AuPtPd/ASA and PtPd/ASA catalysts are mesoporous materials possessing non-uniform pore sizes and shapes. Contrary to those catalysts, the PtPd/MWNT catalyst display isotherm of

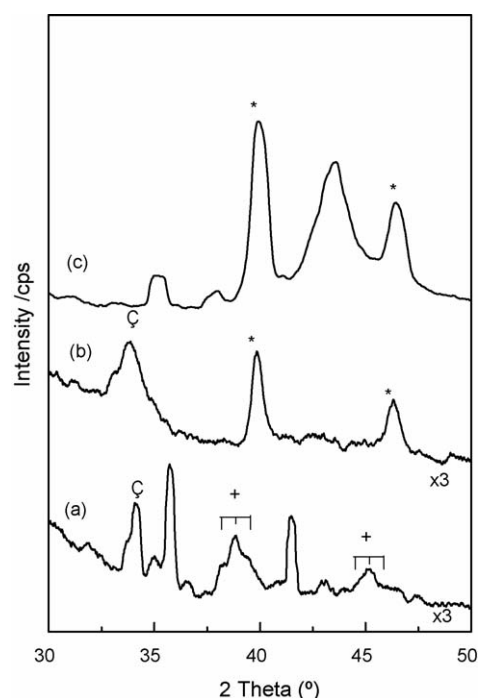


Fig. 1. X-ray patterns of the oxide AuPtPd/ASA (a), PtPd/ASA (b) and PtPd/MWNT (c) catalysts; (\*)  $\text{Pt}^0$  or  $\text{Pd}^0$ ; (+) Au and Au alloyed with Pd; (c) PdO or PtO phases.

Type II with a H3-type hysteresis loop [33,41], indicating that this is macroporous material having non-rigid slit-shaped pores. Table 1 compiles the BET specific areas and the average pore size of the catalysts. The AuPtPd/ASA catalyst showed a largest BET specific area and a lowest average pore size among the catalysts studied. As expected, the PtPd/MWNT catalyst showed a much lower BET specific area and a larger average pore size than the ASA-supported catalysts.

The XRD patterns of the oxide catalysts are shown in Fig. 1. The results of the XRD analysis are summarized in Table 1, in which the different crystal phases along with the corresponding molar percentages of the species are listed. As expected from the PVP method employed as well from use of the ternary formulation, the XRD pattern of the Au-promoted PtPd/ASA catalyst shown in Fig. 1 (diffractogram (a)) is much more complicated than those of binary PtPd/ASA and PtPd/MWNT catalysts prepared by impregnation (diffractograms (b) and (c), respectively). Through the fitting of the main reflection peaks, the evaluation of the lattice parameters allowed the metallic atomic composition of the AuPd solid solution formed in the ternary sample. After Gaussian deconvolution, the peak indicative of the species containing gold revealed three peaks at  $38.18^\circ$ ,  $38.74^\circ$  and  $39.27^\circ$  reflections, which correspond to  $\text{Au}^0$  (JCPDS 4-784),  $\text{Au}_{70}\text{Pd}_{30}$  alloy (28%) and  $\text{Au}_{42}\text{Pd}_{58}$  (57%), respectively; both the latter derived from the angular shift of the main reflection lines of the Au (1 1 1) ( $2\theta = 38.18^\circ$ ) and Pd (1 1 1) phases ( $2\theta = 40.12^\circ$ ). The AuPtPd/ASA catalyst also shows a reflection peak at  $34.0^\circ$ , which may be due to PtO (JCPDS 85-0714) and/or PdO (JCPDS 85-0624) phases.

The oxide PtPd/MWNT sample shows the reflection peaks typical of  $\text{Pd}^0$  (JCPDS 46-1043; Pd (1 1 1);  $2\theta = 40.12^\circ$ ) and the

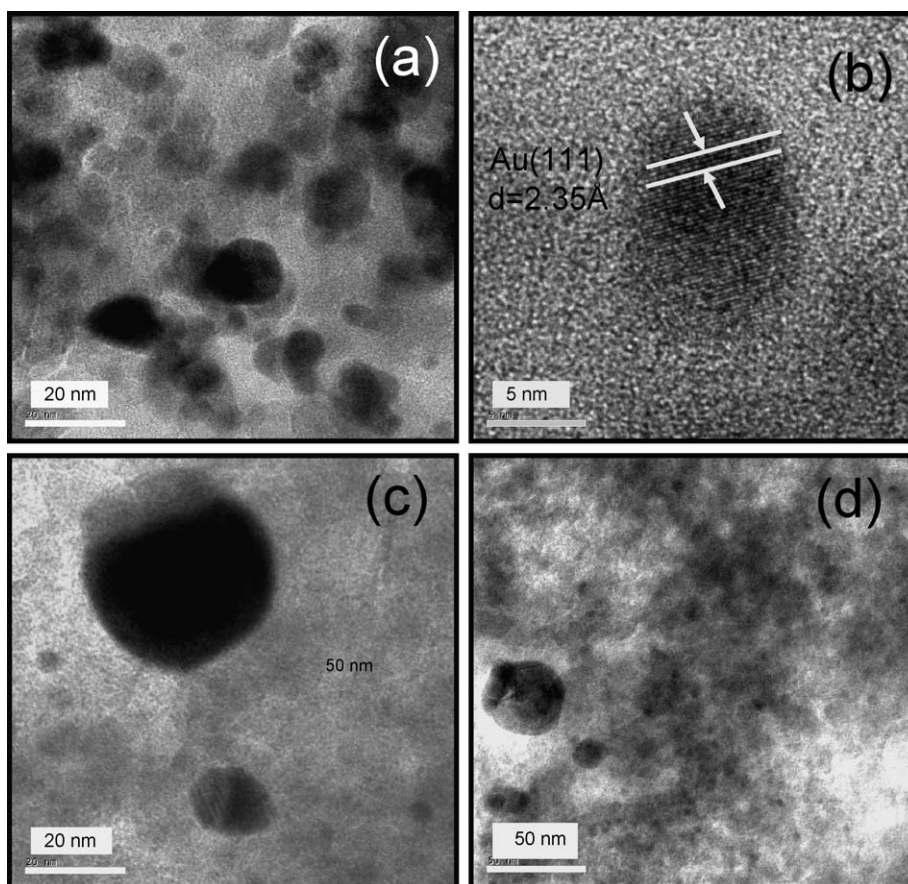


Fig. 2. Electron micrographs of the ASA-supported catalysts after reduction at 573 K: (a) TEM and (b) HRTEM of AuPtPd/ASA, (c) and (d) TEM of PtPd/ASA.

PtPd alloy phase ( $2\theta = 39.9^\circ$ ), the latter derived from the angular shift of the Pt (1 1 1) and Pd<sup>0</sup> (1 1 1) main reflection lines at  $2\theta = 39.76^\circ$  and  $40.12^\circ$ , respectively. The molar composition of the PtPd alloy was calculated as Pt<sub>48</sub>Pd<sub>52</sub>. As the Pt/Pd molar ratio is 1, Pt<sup>0</sup> particles with sizes below ca. 4 nm, which are not detected by XRD, are also present on the surface of MWNT. On the other hand, the PtPd/ASA catalyst exhibited Pt<sup>0</sup> (JCPDS 04-802;  $2\theta = 39.76^\circ$ ), PtO (JCPDS 85-0714) and/or PdO (JCPDS 85-0624) phases, both the latter deduced from the reflection peak at  $34.0^\circ$ . Contrary to PtPd/MWNT, the PtPd/ASA catalyst did not show evidence of PtPd alloy formation probably due to different metal precursors employed in the catalyst preparation. Indeed, our previous work on the 0.3% Pt–1% Pd/ASA catalyst prepared using H<sub>2</sub>PtCl<sub>6</sub> and Pd(NO<sub>3</sub>)<sub>2</sub> as metal precursors confirmed PtPd alloy formation on this sample [7]. Similarly, PtPd alloy formation for the PtPd/ASA catalyst prepared from PtCl<sub>2</sub> and PdCl<sub>2</sub> precursors was reported by Fujikawa et al. [42]. Considering the very low metal loadings in all samples (ca. 0.7 wt.% for both Pt and Pd, and 0.3 wt.% for Au) and the low resolution of the XRD diffractograms, no attempt was made for the calculation of the particle's size by the Debye–Scherrer equation. Thus, phase assignments can only be considered as a rough estimation.

Due to limitation of XRD measurement, the reduced (573 K) catalysts were characterized by electron microscopy. The TEM

images of the reduced AuPtPd/ASA are presented in Fig. 2(a) and (b) whereas those of the PtPd/ASA sample are shown in Fig. 2(c) and (d). It is clearly seen that the low magnification TEM image of the ternary sample exhibited smaller metal particles than those of binary counterpart. The main particle size of the AuPtPd/ASA and PtPd/ASA calculated from particle size distribution (not shown here) were 22.0 and 27.9 nm, respectively. For a more precise analysis, the high resolution TEM image of AuPtPd/ASA sample is presented in Fig. 2(b). The Au<sup>0</sup> particles with crystalline lattice (1 1 1 planes) and distance ca. 0.235 nm are observed. The stabilization of gold in small clusters is difficult due to the low melting point of Au [43], thus the observed Au<sup>0</sup> particle is relatively large (ca. 9.6 nm). Compared to PtPd/ASA sample, the TEM images of the PtPd/MWNT sample showed a more homogeneous metal dispersion (not shown here). For the latter sample, the calculated main metal particle size is ca. 7.8 nm.

The CO uptake values of the catalysts after reduction at 573 K, as derived from volumetric CO chemisorption measurements, are shown in Table 2. For the CO uptake values, the observed trend is: PtPd/ASA > PtPd/MWNT > AuPtPd/ASA. The lower extent of CO adsorption on AuPtPd/ASA is due to the fact that CO is only sparingly adsorbed on Au<sup>0</sup> [16]. Since the TEM results of the reduced AuPtPd/ASA indicate a more homogeneous metal dispersion than in the reduced PtPd/ASA, it can

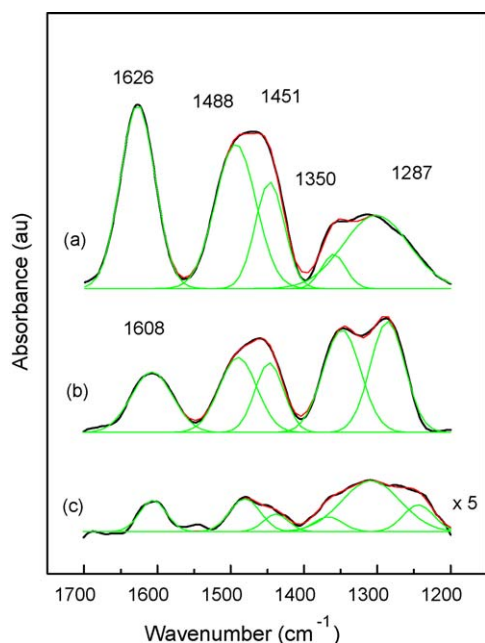


Fig. 3. DRIFTS spectra (at room temperature) of the adsorbed species arising from the adsorption of  $\text{NH}_3$  over pre-reduced (573 K) binary PtPd catalysts: PtPd/ASA (a); AuPtPd/ASA (b); PtPd/MWNT (c).

be inferred that the decrease in CO chemisorption capacity of the former catalyst with respect to the latter is due to the decoration of the Pt/Pd particles by some Au species. Because CO molecules can be adsorbed on the PtPd alloy of PtPd/MWNT sample in both linear and bridge forms, and because there are striking differences in site preference and adsorption structures between the Pt and Pd surfaces [44,45], no attempt was made to calculate the metal dispersion and average metal particle size from the CO chemisorption data.

The acidity of the pre-reduced (at 573 K) catalysts was studied by DRIFT spectroscopy of  $\text{NH}_3$  adsorption at room temperature (reversible adsorption). Fig. 3 shows the DRIFTS- $\text{NH}_3$  spectra of the catalysts studied. As seen, all catalysts show one band at  $1626\text{ cm}^{-1}$  and two broad bands, which after splitting show two set of bands: one at 1488 and  $1451\text{ cm}^{-1}$  and the other at 1352 and  $1287\text{ cm}^{-1}$ . The band with maxima observed at ca.  $1626\text{ cm}^{-1}$  is due to ammonia adsorbed onto Lewis acid surface sites ( $\delta_{\text{asy}}(\text{NH}_3)$ ). For AuPtPd/ASA and PtPd/MWNT, this band is shifted toward the lower frequency region (from  $1626$  to  $1610\text{ cm}^{-1}$ ) and it is much less intense than in case of the PtPd/ASA catalyst. For all catalysts, the band at  $1451\text{ cm}^{-1}$  could be ascribed to Brønsted-bonded  $\text{NH}_4^+$  species ( $\delta_{\text{asy}}(\text{NH}_4^+)$ ) whereas the band at  $1488\text{ cm}^{-1}$  could be attributed to bending mode of  $\text{NH}_2$  surface species adsorbed on a Pd/Pt [46]. Finally, the two overlapping bands with maxima at 1287 and  $1352\text{ cm}^{-1}$  are linked with Lewis acid sites ( $\delta_{\text{asy}}(\text{NH}_3)$ ) and an amino cation ( $\text{H}_2\text{N}^+$ ), respectively [47]. Considering the intensity of the peak at ca.  $1451\text{ cm}^{-1}$ , determined after Gaussian deconvolution of the spectra, the Brønsted acidity of the catalysts follows the trend: PtPd/ASA > AuPtPd/ASA  $\gg$  PtPd/MWNT. The same trend is followed by the Brønsted-to-Lewis (B/L) acidity ratio in Table 2,

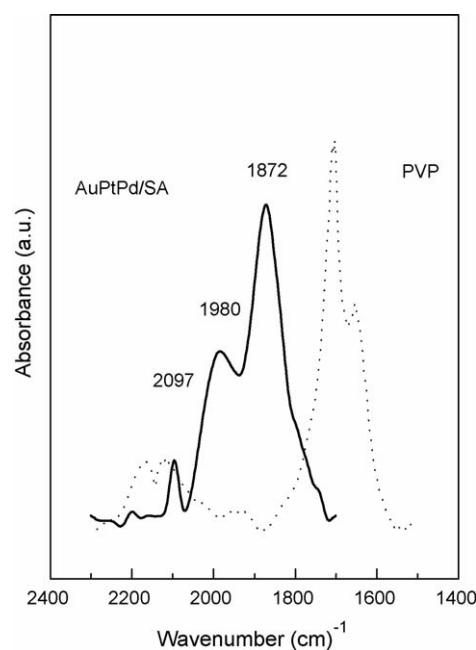


Fig. 4. FTIR spectra (at room temperature) of the CO adsorbed on the pre-reduced (573 K) ternary AuPtPd/ASA catalyst: irreversible adsorption. For comparison, the spectra of poly(*N*-vinyl-2-pyrrolidone) (PVP) is included (dotted line).

as determined from the intensity of the bands at ca. 1450 and  $1300\text{ cm}^{-1}$ , respectively. Thus, after addition of Au to the PtPd formulation both Brønsted and Lewis acidities decreased, but the AuPtPd/ASA sample still had a higher B/L acidity ratio than PtPd/MWNT.

The nature of surface sites on the ternary AuPtPd/ASA catalyst after its activation in hydrogen at 573 K was shown by FTIR of adsorbed CO. The FTIR-CO spectra of this catalyst together with the spectra of the as-received poly(*N*-vinyl-2-pyrrolidone) compound are displayed in Fig. 4. Comparisons of both spectra clearly indicate that the bands are not due to the residual presence of PVP on the surface. The IR spectrum of the AuPtPd/ASA catalyst showed the small band at  $2099\text{ cm}^{-1}$  and a broad and strong band centred at  $1872\text{ cm}^{-1}$ , with a tail towards the lower frequency region, together with an overlapped band around  $1980\text{ cm}^{-1}$ . Based on the data found in the literature and in keeping with the XRD data (Table 1), the band at  $2099\text{ cm}^{-1}$  can be assigned to CO linearly adsorbed on  $\text{Pd}^0$  sites [16] whereas the bands at 1980 and  $1872\text{ cm}^{-1}$  should be ascribed to multibonded CO species bridging over  $\text{Pd}^0$  clusters [48] and/or adsorbed on different metal sites such as terraces, steps or kink sites of the  $\text{Au}_{70}\text{Pd}_{30}$  and  $\text{Au}_{42}\text{Pd}_{58}$  alloys. No peaks ascribed to CO adsorbed on  $\text{Pt}^0$  species (CO linear band at ca.  $2070\text{ cm}^{-1}$ ) and platinum species in an electron-deficient state (CO linear band at  $2080\text{ cm}^{-1}$ ) [37] were observed. Finally, although XRD showed the presence of  $\text{Au}^0$  clusters on the surface of AuPtPd/ASA, neither bands due to CO linearly adsorbed on reduced gold sites (ca.  $2127\text{ cm}^{-1}$ ) nor multisite CO adsorption on  $\text{Au}^0$  particles (ca.  $2043\text{ cm}^{-1}$ ) [49] were observed. The absence of these bands is likely due to removal of weakly adsorbed CO molecules upon degassing at room temperature.

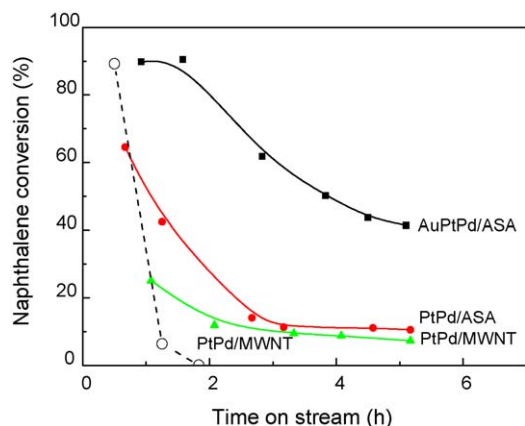


Fig. 5. Time-on-stream behavior of the ASA- and MWNT-supported catalysts in naphthalene hydrogenation (solid line) at  $T=448$  K,  $P=2.0$  MPa and  $WHSV=45.7$  h $^{-1}$ . The time-on-stream behavior of the PtPd/MWNT catalyst in benzene hydrogenation in the presence of 1-butanethiol (dot line) ( $T=408$  K;  $P=2.0$  MPa,  $WHSV=39.6$  h $^{-1}$ ) is also shown.

### 3.2. Naphthalene hydrogenation

The conversion of naphthalene ( $T=448$  K,  $P=2.0$  MPa and  $WHSV=45.7$  h $^{-1}$ ) obtained for all catalysts are given in Fig. 5 as a function of time on-stream (TOS). As seen in this figure, during whole time on-stream operation, naphthalene conversion follows a trend of AuPtPd/ASA  $\gg$  PtPd/ASA  $>$  PtPd/MWNT. The initial naphthalene conversion calculated from extrapolation of data at TOS=0 were about 100% (AuPtPd/ASA), 90% (PtPd/ASA) and 40% (PtPd/MWNT). Thus, the AuPtPd/ASA catalyst proved to be the most active among those studied, by far exceeding the performance of both binary PtPd/ASA and PtPd/MWNT catalysts. The naphthalene conversion was found to increase with increasing reaction temperature from 448 to 483 K (Table 3).

In order to compare the intrinsic activity of catalysts in the absence of catalyst deactivation, Fig. 6 shows the initial turnover frequency (TOF's) calculated from the reaction rates at TOS=0 h and the number of exposed surface metal atoms (derived from CO chemisorption and TEM). As seen in Fig. 6, the initial TOFs values calculated taking account the number of exposed surface atoms follow the order: AuPtPd/ASA  $\gg$  PtPd/ASA = PtPd/MWNT whereas those calculated taking account the main particle size follow the trend: AuPtPd/ASA  $>$  PtPd/MWNT  $>$  PtPd/ASA. Thus, irrespectively of the method of TOF calculation, the activity is clearly enhanced in the gold-promoted catalyst.

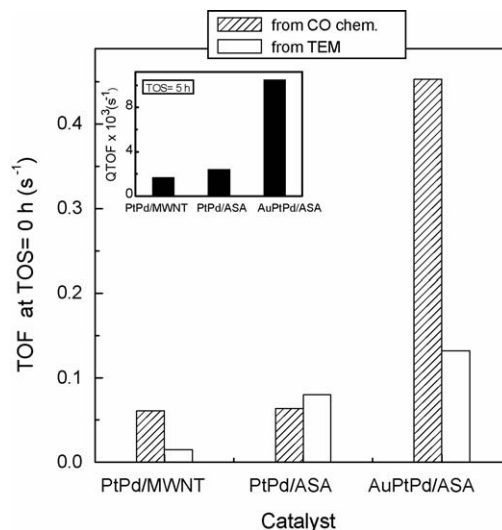


Fig. 6. Comparison of the initial turnover frequency (TOF at TOS=0), as determined by CO chemisorption and also by TEM, and quasi-turnover frequency (QTOF at TOS=5 h, inset of this figure) for the naphthalene hydrogenation over ASA- and MWNT-supported catalysts. Reaction conditions were:  $T=448$  K,  $P=2.0$  MPa,  $WHSV=45.7$  h $^{-1}$ .

Taking into account that all the catalysts showed deactivation during on-stream operation (Fig. 5), it might be expected that metal accessibility after 5 h on-stream operation would be much lower than those deduced from the CO chemisorption data of the fresh reduced catalysts. Thus, for steady-state conditions the quasi-turnover frequency (QTOF) values were calculated from the specific reaction rates expressed as moles of molecules converted per second and per moles of Pt and Pd. The QTOF values of all catalysts are compared in the inset of Fig. 6. As seen in this figure, the specific reaction rates at TOS=5 h follows the trend: AuPtPd/ASA  $\gg$  PtPd/ASA  $>$  PtPd/MWNT, indicating again that the activity is clearly enhanced in the gold-promoted catalyst. This trend did not change when the QTOF value of AuPtPd/ASA catalyst was calculated considering the moles of Au.

Fig. 7 shows the Arrhenius plots of naphthalene HYD at 448, 463 and 483 K. As seen in this figure, the ternary AuPtPd catalyst shows temperature-independent  $E_a$ , but the binary catalysts exhibit a strong increase of  $E_a$  at the highest reaction temperature. Since the overall apparent activation energy is a composite parameter including adsorption terms, an increase in  $E_a$  with increasing temperature might indicate absence of the catalyst stability at high reaction temperatures.

Table 3

Activity and selectivity in the reaction of naphthalene HYD over the AuPtPd/ASA, PtPd/ASA and PtPd/MWNT catalysts<sup>a</sup>

Catalyst	$E_a^b$ (kJ/mol)	Conv. (%)	Sel. tetralin (%)	Sel. decalin (%)	<i>Cis/trans</i> -decalin ratio
AuPtPd/ASA	78.3	43.7 (92.6)	94.8	5.2	0.7
PtPd/ASA	78.2	11.3 (40.6)	78.8	21.2	1.1
PtPd/MWNT	66.2	8.7 (27.4)	97.0	3.0	0.9

<sup>a</sup> Naphthalene conversion, selectivity toward tetralin and decalin, and the *cis*-decalin-to-*trans*-decalin ratio for the reaction of naphthalene HYD at  $T=448$  K,  $P=2.0$  MPa,  $WHSV=45.7$  h $^{-1}$  and steady-state conditions. Naphthalene conversion at 483 K is given in parenthesis.

<sup>b</sup> Apparent activation energy as calculated from the Arrhenius plot. Reaction conditions were:  $T=448$ – $463$ – $483$  K;  $P=2.0$  MPa;  $WHSV=45.7$  h $^{-1}$ .

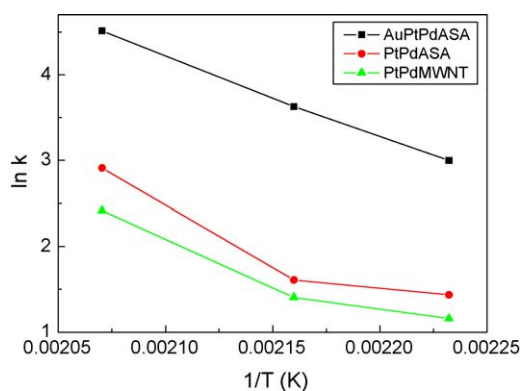


Fig. 7. Arrhenius plots for HYD of naphthalene on the catalysts. Reaction conditions were:  $T = 448\text{--}463\text{--}483\text{ K}$ ,  $P = 2.0\text{ MPa}$ ,  $\text{WHSV} = 45.7\text{ h}^{-1}$ , steady-state data.

The apparent activation energy ( $E_a$ ) values of the catalysts are summarized in Table 3. As seen, both ASA-supported catalysts show a similar  $E_a$  values ( $78.2\text{--}78.3\text{ kJ mol}^{-1}$ ), which are significantly higher than those of the PtPd/MWNT catalyst ( $66.1\text{ kJ mol}^{-1}$ ). The higher  $E_a$  over ASA-supported catalysts indicates that the energetics for the reaction is less favorable than in case of MWNT-supported sample. Thus, the high activity of the AuPtPd/ASA catalyst can be accounted for by the pre-exponential factor, rather than by the activation energy.

### 3.2.1. Product distribution in naphthalene HYD

It is well known that naphthalene hydrogenation is a consecutive reaction: naphthalene  $\rightarrow$  tetralin (1,2,3,4-tetrahydronaphthalene)  $\rightarrow$  decalin (*cis* and *trans* decahydronaphthalene) [2], 1,9-octalin (octa-hydro-naphthalene) being the most reactive intermediate product of the conversion of tetralin to decalin [50]. Tetralin is formed relatively easy, whereas the hydrogenation of the common double bond is slow and critical and is followed by rapid saturation to decalin. From the viewpoint of reduction of particulate matters in diesel exhaust, decalin is more favorable than tetralin.

The selectivity toward tetralin and decalin as well as the *cis/trans*-decalin ratio in reaction at 448 K are compiled in Table 3. All catalysts showed a strong selectivity toward tetralin formation (in range 78.8–97.0% at 448 K). This is probably because Pd has the unique ability to stop naphthalene hydrogenation to tetralin formation [50]. No high cetane number's products derived from hydrogenolysis/ring-opening reactions (such as alkylbenzenes, alkylcyclohexanes, methylindanes and methylindenes, spyrodecane) were detected. This is expected

since metallic Pt/Pd show relatively low activity for cleaving unsubstituted C–C bonds [3,4]. The very small selectivity toward decalin observed for all catalysts is probably because tetralin hydrogenation to decalin do not have sufficient time to occur due to a very low contact time employed (0.022 h) and competitive adsorption of naphthalene and tetralin on the active sites [51]. Indeed, the naphthalene hydrogenation over Pt/TiO<sub>2</sub> demonstrated that naphthalene interacts with surface metals more strongly than tetralin and prevents the hydrogenation of tetralin to decalin [52].

It is known that the formation of the *cis*-decalin isomer is favored by all metals and results from the addition of hydrogen from the same side across the double bond common to the two rings, e.g., from the metal to the molecule arranged in a flat position on the surface [53]. For the PtPd/ASA and PtPd/MWNT catalysts, the *cis/trans*-decalin ratio of 1.1 and 0.9, respectively, suggests a less inhibited presence of the 1,8-octalin intermediate adsorbed with the hydrogen atom in position 10 facing the Pt<sup>0</sup>/Pd<sup>0</sup> surfaces. On the contrary, for AuPtPd/ASA catalyst the low *cis/trans*-decalin ratio of 0.7 indicates that *cis*-decalin isomerization is affected by site competition with other molecules present in the feed.

### 3.2.2. Catalyst deactivation in reaction of naphthalene HYD

For steady-state conditions, the ternary AuPtPd/ASA catalyst displays the largest naphthalene conversion whereas PtPd/ASA catalyst shows a very similar catalytic behavior to that of PtPd/MWNT counterpart (Fig. 5). This is, in part, because the catalysts suffer a different degree of the catalyst deactivation during on-stream operation. The percentage of catalyst deactivation in reaction at 448 K, as calculated from equation  $[(X_{1h} - X_{5h})/X_{1h}] \times 100\%$ , is offered in Table 4. The deactivation percentage increased in the order AuPtPd/ASA (53.9%) < PtPd/MWNT (70.9%) < PtPd/ASA (83.7%). Thus, the best catalytic performance of the ternary sample in the HYD of naphthalene must partly be due to its lower deactivation during on-stream operation.

In order to shed light on the origin of catalyst deactivation during naphthalene HYD, TGA analysis was employed. This technique confirmed that the main catalyst deactivation in naphthalene HYD was due to deposition of carbonaceous residues/coke on the catalyst surface. As a consequence, the availability of hydrogen on metal sites becomes lower [54]. Since the extent of catalyst deactivation is influenced by the acid sites of the support [55,56], a drop in their

Table 4  
Results of TGA analysis of the catalysts after the HYD of naphthalene<sup>a</sup>

Catalyst	Deac. <sup>b</sup> (%)	Amount of burnt species (%)				
		<500 K, C-residues	500–650 K, naphthalene	650–700 K, coke	>700 K, MWNT	Total mass loss <700 K
AuPtPd/ASA	53.9	23.1	1.8	1.8	–	26.7
PtPd/ASA	83.7	1.3	0.5	2.0	–	3.8
PtPd/MWNT	70.9	1.6	2.3	7.4	66.3	11.3

<sup>a</sup> Reaction conditions were:  $T = 448\text{ K}$ ,  $P = 2.0\text{ MPa}$ ,  $\text{WHSV} = 45.7\text{ h}^{-1}$  and  $\text{TOS} = 5\text{ h}$ .

<sup>b</sup> Catalyst deactivation as calculated from equation  $[(X_{1h} - X_{5h})/X_{1h}] \times 100\%$ , where X is naphthalene conversion.

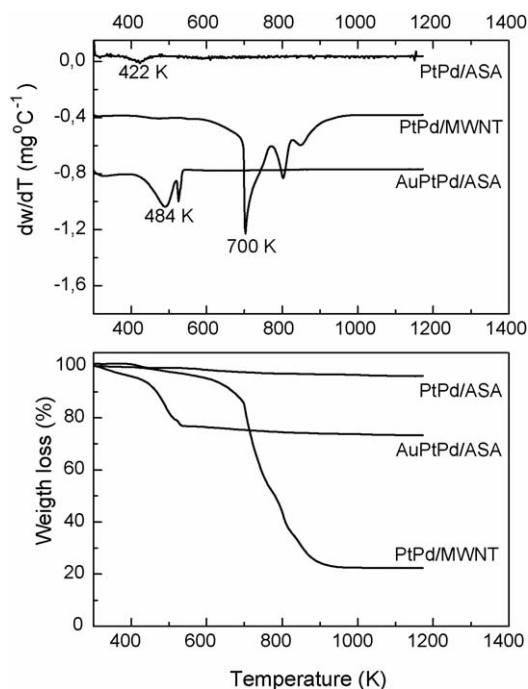


Fig. 8. DTA and TGA profiles of the catalysts tested in the HYD of naphthalene at  $T = 448$  K,  $P = 2.0$  MPa and  $WHSV = 45.7$  h<sup>-1</sup>.

amount during on-stream operation is expected to occur (see Fig. 5).

The weight change during oxidation of the used catalysts in a 20% O<sub>2</sub>/N<sub>2</sub> mixture (DTA and TGA profiles) is shown in Fig. 8. The experimental  $dW/dT$  (mg K<sup>-1</sup>) curves were analyzed by a mathematical fitting program and were deconvoluted into Gaussian functions (not shown here). The percentages of total mass loss corresponding to different burnt species are shown in Table 4. Thus, the TGA peaks in temperature ranges below 500 K, 500–650 K, and below 700 K can be ascribed to the burning of carbonaceous residues, naphthalene and coke, respectively. Burning of the MWNT support occurs at temperatures above 700 K. The region below 500 K cannot be unambiguously explained, since it lies within the region where the reactant mixture might be desorbed. The second region (500–650 K) is associated with the naphthalene/tetralin desorption since no reaction would occur under these conditions. In the case of naphthalene/tetralin desorption, the

observed trend was PtPd/MWNT > AuPtPd/ASA > PtPd/ASA. The amount of burnt coke follows a trend of AuPtPd/ASA (1.8%) ≈ PtPd/ASA (2.0%) ≪ PtPd/MWNT (7.4%), whereas the burning of carbonaceous residues followed a sequence of AuPtPd/ASA (23.1%) ≫ PtPd/MWNT (1.6%) ≈ PtPd/ASA (1.3%). The larger carbonaceous residues formation on the ternary sample than on binary catalysts could be interpreted on the basis that a lower surface concentration of dissociated hydrogen is present on the AuPtPd/ASA catalyst, and therefore it is unable to hydrogenate the adsorbed carbonaceous residues formed by side reactions. On the contrary, for the PtPd/ASA and PtPd/MWNT catalysts the hydrogen dissociation on their metal sites might occur. The largest naphthalene conversion decay during on-stream operation at 448 K over PtPd/ASA (Fig. 5) is in good agreement with its largest acidity as determined by DRIFT-NH<sub>3</sub> (Fig. 3). Moreover, as this catalyst shows the largest selectivity toward decalin formation (21.2% at 448 K), its low naphthalene conversion at 448 K and TOS = 5 h could be linked with the stronger tetralin adsorption on the metal sites limiting naphthalene adsorption on those sites. The close correlation observed in this study between decalin formation and naphthalene conversion decay confirms that the decrease in tetralin formation is a more sensitive index of the catalyst deactivation than a decrease in naphthalene conversion [24].

### 3.2.3. X-ray photoelectron spectroscopy (XPS) of the used samples

Table 5 lists the position of the noble metals' photoelectron lines together with various molar ratios of key surface elements. Fig. 9 shows the Pd 3d core-level XPS spectra. As seen in this figure, contrary to the PtPd/MWNT sample, both the PtPd/ASA and AuPtPd/ASA catalysts show the unique peak in which BE coincides with that observed for metallic palladium (335.0 eV and 335.8 eV, respectively) [57]. The Pd 3d core-level spectra of the used PtPd/MWNT catalyst show two peaks: one at ca. 335.5 eV, indicative of Pd<sup>0</sup> species [57], and another less intense peak at 337.0 eV, which is attributable to some residual PdCl<sub>2</sub>(H<sub>2</sub>O)<sub>2</sub> species [58] originated by the use of chloride precursors. Taking into account the percentage of palladium species shown in parenthesis in Table 5, the amounts of Pd<sup>0</sup> and PdCl<sub>2</sub>(H<sub>2</sub>O)<sub>2</sub> species are 62% and 38%, respectively.

Table 5  
Binding energies (eV) of core electrons and surface atomic ratios (XPS) of used catalysts<sup>a</sup>

Catalyst	Pd 3d <sub>5/2</sub>	Pt 4d <sub>5/2</sub>	Pt 4f <sub>7/2</sub> (Au 4f <sub>7/2</sub> )	Pd/Al(C) <sup>b</sup> at × 10 <sup>3</sup>	Pt/Al (C) <sup>b</sup> at × 10 <sup>3</sup>	Au/Al <sup>b</sup> at × 10 <sup>3</sup>
AuPdPt/ASA, naphthalene HYD	335.2	314.1	(84.0)	156 (11)	65 (7)	50 (2.8)
PdPt/ASA, naphthalene HYD	335.0	314.4	–	52 (13)	7 (7)	–
PtPd/MWNT, naphthalene HYD	335.5 (62), 337.0 (38)	–	71.6 (69%), 74.2 (31%)	1.3 (0.8)	0.9 (0.5)	–
PtPd/MWNT <sup>c</sup> , benzene HYD (+S) <sup>c</sup>	335.8	–	71.7	1.7	0.8	–
PtPd/MWNT <sup>d</sup> , red. in H <sub>2</sub> at 573 K	335.4 (70), 337.0 (30)	–	71.5 (67%), 73.5 (33%)	3.3	1.7	–

<sup>a</sup> After naphthalene hydrogenation at  $T = 483$  K,  $P = 2.0$  MPa and  $WHSV = 45.7$  h<sup>-1</sup>. The percentages of the components are given in parenthesis.

<sup>b</sup> The bulk Pt(Pd)/Al(C) and Au/Al atomic ratios based on chemical analysis data are given in parenthesis.

<sup>c</sup> After benzene HYD in the presence of 1-butanethiol at  $T = 408$  K,  $P = 2.0$  MPa and  $WHSV = 39.6$  h<sup>-1</sup>.

<sup>d</sup> After reduction at 573 K.

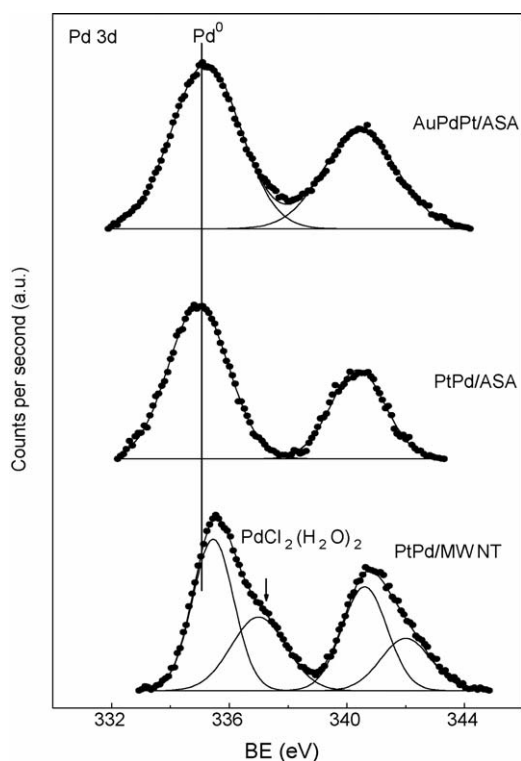


Fig. 9. Pd 3d core-level spectra of the catalysts after naphthalene HYD.

For the PtPd/MWNT catalyst, the energy region of intense Pt  $4f_{7/2}$  core level was recorded. Since for ASA-supported catalysts the Pt  $4f_{7/2}$  energy region became overshadowed by the presence of a very strong Al 2p peak, the energy region of the less intense Pt 4d peak was recorded together with the energy regions of Si 2p, Al 2p and Pd  $3d_{5/2}$  core levels. Regarding the Pt  $4f_{7/2}$  core level, after naphthalene HYD the PtPd/MWNT catalyst exhibits two components, one at a BE of 71.6 eV and the other at a BE 74.2 eV, assigned to Pt<sup>0</sup> and Pt<sup>2+</sup> ions in the close vicinity of chloride anions, respectively [57]. Contrary to the PtPd/MWNT sample, the peak indicative of the latter species is absent in the spectra of the spent ASA-supported catalysts, which only show a peak around 314.1–314.4 eV, indicating the formation of Pt<sup>0</sup> species [57]. Additionally, the AuPtPd/ASA catalyst shows the BE of Au  $4f_{7/2}$  peak at 84.0 eV indicative of Au metal particles.

The quantitative XPS analyses of the PtPd/MWNT and both ASA-supported catalysts are shown in Table 5. The surface exposure of platinum and palladium species, derived from the Pt/Al(C) and Pd/Al(C) atomic ratios, respectively, follows the trend: AuPtPd/ASA  $\gg$  PtPd/ASA > PtPd/MWNT. Thus, the AuPtPd/ASA sample exhibits the largest surface concentration of both metals among the catalysts. The comparison of Pt/Al(Pt/C) and Pd/Al(Pt/C) ratios with the bulk ones (given in Table 5 in parenthesis) points out to the preferential segregation of the metals on the surface of both ASA and MWNT substrates. For all catalysts, the XPS Pt/Pd atomic ratios in range 0.135–0.69 suggested a larger Pd than Pt surface exposure. Finally, since the Au/Al value from the XPS analysis is much higher than that of the bulk atomic ratio (0.05 versus 0.028), Au is mainly located on the outer catalyst surface.

Table 6

Activity and selectivity data for simultaneous naphthalene and toluene HYD and HDS of DBT over the AuPtPd/ASA catalyst

	Temperature (K)		
	523	548	573
DBT conv. (%)	100	100	100
Toluene conv. (%)	1.2	2.07	5.4
NP conv. (%)	100	100	100
Sel. tetralin (%)	94.0	85.3	72.6

<sup>a</sup>Reaction conditions:  $T=523\text{--}548\text{--}573$  K,  $P=2.0$  MPa; WHSV = 41.2 h<sup>-1</sup>; steady-state data.

### 3.3. Aromatics HYD in the presence of S-compounds

Since the principal characteristics of a catalyst to be used in a second step of the hydrotreating unit are high hydrogenation activity and S-resistance, the AuPtPd/ASA catalyst was tested in a reaction employing model feed approaching the composition of Light Gas Oil (LGO): toluene, naphthalene and DBT (S = 100 ppm). The naphthalene, toluene and DBT conversions over this catalyst are shown in Table 6, together with selectivity toward tetralin. Under the reaction conditions employed ( $T=523\text{--}548\text{--}573$  K,  $P=2.0$  MPa and WHSV = 41.2 cm<sup>-1</sup>), naphthalene and DBT transformations over AuPtPd/ASA catalyst were total. In contrast, the low toluene conversion (in range 1.2–5.4%) indicates that toluene HYD is much more difficult than that of naphthalene. This is related to a decrease in the resonance energy per aromatic ring as well as to differences in the  $\pi$ -electron cloud density in the aromatic ring as result of the inductive effect of the methyl group [59]. As seen in Table 6, an increase in temperature from 523 to 573 K led to an increase in toluene conversion over AuPtPd/ASA. Simultaneously, the selectivity toward decalin formation in naphthalene HYD increased. Since the deep hydrogenation from tetralin to decalin is more sulfur-sensitive than that of partial hydrogenation [60], the increase in both toluene conversion and selectivity toward decalin are only possible in case of S-tolerance of the AuPtPd/ASA catalyst. The S-tolerance of this catalyst was confirmed also by XPS measurements (results not shown here).

To confirm the easy S-poisoning, the PtPd/MWNT catalyst was tested in the reaction of benzene HYD in the presence of 1-butanethiol (5 ppm of S). Since the larger S-resistance of PtPd/ASA catalyst in comparison with PtPd/MWNT sample was confirmed by us previously in the simultaneous naphthalene and toluene hydrogenation in the presence of DBT (100 ppm of S;  $T=498$  K,  $P=5.0$  MPa, WHSV = 25.8 h<sup>-1</sup>) [33], the larger S-resistance of the former is also assumed in this study. Fig. 5 shows a comparison of the on-stream behavior of PtPd/MWNT catalyst in a reaction without S (naphthalene HYD) with that in the presence of S (benzene HYD). Contrary to naphthalene HYD, the PtPd/MWNT catalyst undergoes a rapid deactivation during benzene HYD in the presence of 1-butanethiol ( $T=408$  K,  $P=2.0$  MPa and WHSV = 39.6 h<sup>-1</sup>). The S-poisoning of active sites was confirmed by XPS measurements. As seen in Table 5, with respect to naphthalene HYD, the PtPd/MWNT used in benzene HYD (+S) shows a shift in binding

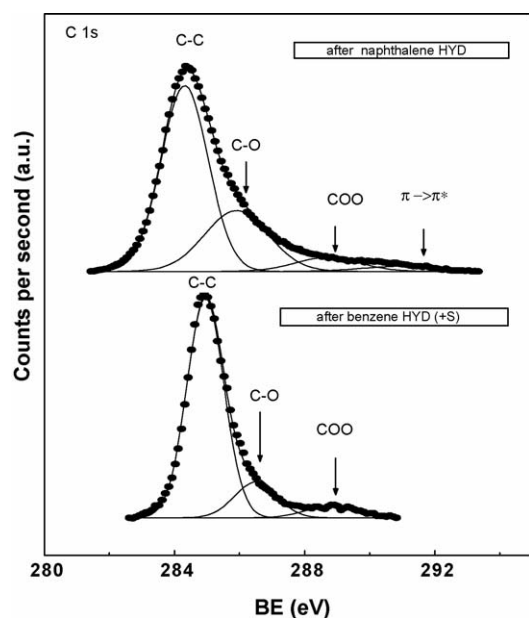


Fig. 10. C 1s core-level XPS spectra of the PtPd/MWNT catalyst after hydrogenation of naphthalene and benzene hydrogenation in the presence of 1-butanethiol.

energy of Pd 3d<sub>5/2</sub> peak (from 335.5 to 335.8 eV). This shift is observed also with respect to the binding energy of the Pd 3d<sub>5/2</sub> peak of the fresh reduced PtPd/MWNT (335.4 eV). This positive energy shift might indicate the loss of metallic character of Pd. The formation of Pd(Pd)S compounds might well occur, as it was confirmed in our previous study [33], but it cannot be seen by XPS owing to the very low photoionization cross-section of the S 2p level peak as well as the decomposition of the weakly bonded S on the surface of Pt/Pd crystallites during the vacuum pretreatment carried out within the pretreatment/analysis chambers of the spectrometer [61].

More information about secondary effect of S-poisoning was obtained by comparing the C 1s level spectra of the PtPd/MWNT after naphthalene HYD and benzene HYD in the presence of 1-butanethiol. In Fig. 10, the C 1s core-level spectra have been fitted to several symmetric components. The main peak at 284.9 eV is unambiguously assigned to the C 1s of graphitic carbon [62]. This peak shows a larger peak half-width (eV) after naphthalene HYD than after benzene HYD (1.8 versus 1.6 eV) suggesting the larger heterogeneity of the phases on the MWNT surface after naphthalene than after benzene HYD, in good agreement with the absence of Pt<sup>2+</sup>/Pd<sup>2+</sup> species in close vicinity with Cl<sup>-</sup> ions observed after benzene HYD (Table 5). In Fig. 10 the shoulder of the main peak is composed of two peaks, which are assigned to the C 1s of C–O bonds (286.5 eV) and the carboxyl carbon –COOH (288.8 eV) [62]. These oxygen-containing carbon groups were developed during the oxidative treatment of the MWNT material with HNO<sub>3</sub> and also during incorporation of metal precursors [33]. After naphthalene HYD the functional groups containing hydroxyl and carboxyl carbon represented 39% and 11% whereas after benzene HYD (+S) their percentages were 15% and 6%, respectively. Thus, besides the S-poisoning of the metal sites, the drastic drop in activity

of the PtPd/MWNT catalyst is connected with a large decrease in amount of both CO– and COO– groups, which is probably induced by adsorption of the unreacted benzene molecules on the acid sites of support.

### 3.4. Catalyst activity–structure correlation

The higher activity of the AuPtPd/ASA catalyst in hydrogenation of naphthalene, relative to binary PtPd/ASA and PtPd/MWNT counterparts, may be due to various conjugated effects. The first is the morphology of this sample which from XRD, XPS and HRTEM can be depicted as aggregates of Au<sub>42</sub>Pd<sub>58</sub> and Au<sub>70</sub>Pd<sub>30</sub> alloys located on the external ASA surface together with the isolated large Au<sup>0</sup> and small Pt<sup>0</sup> particles. It should be remarked that, even though the XRD data given in Table 1 refer to the calcined catalysts, they can still be related to the catalytic behavior since, as pointed out previously [16,18], the catalyst hydrogen pretreatment did not produce changes of the Au<sub>x</sub>Pd<sub>y</sub> alloy structure except for a further reduction of the palladium/platinum oxides, which are present also on the surface of oxide AuPtPd/ASA catalyst. The second explanation for the higher activity of the AuPtPd/ASA catalyst in hydrogenation of naphthalene is the greater stability of the active phases during catalyst activation and/or on-stream reaction induced by the PVP preparation method used [14,16]. In this method, metallic nanoparticles were obtained by alcoholic reduction of metallic ions in the presence of a polymeric stabilizer (poly(*N*-vinyl pyrrolidone)) used as the protective agent. As a consequence, the third effect could be linked with the largest surface exposure of Pt/Pd species on the surface of used AuPtPd/ASA (see XPS data in Table 5) and linked with this – a largest amount of the active sites. Since Au shows much lower hydrogenation properties than Pt and Pd due to limited capacity of gold to dissociate H<sub>2</sub> molecules [11], a largest amount of the active sites implies larger hydrogen dissociation as well as easier flat naphthalene adsorption on the active sites than other catalysts studied [63]. This interpretation is supported by a lowest *cis*-to-*trans*-decalin ratio of this catalyst in reaction at 448 K (see Table 5) indicating the inhibition of decalin isomerization by site competition with naphthalene. Moreover, the origin of a substantial increase of the activity observed for ternary AuPtPd/ASA catalyst could be the presence of surface gold, which weakens the adsorption of naphthalene on active sites, thus facilitating product desorption. A similar explanation was proposed in order to explain the large increase in activity observed for acetylene cyclotrimerization over an Au–Pd catalyst with respect to Pd alone [64]. According to literature data bulk gold can already acts as catalyst but it works at higher temperatures than supported Au particles [11]. Thus, the large increase in naphthalene conversion over AuPtPd/ASA (from 43.7% to 92.6%) raising reaction temperature from 448 to 483 K might come, in part, from a relatively large Au<sup>0</sup> particles (Fig. 2(b)). Finally, considering the moderate acidity of AuPtPd/ASA catalyst, the adsorption of aromatics molecules on acid sites of the support located near the interface with the metallic particles and their further hydrogenation by hydrogen spilled over from the metal surface cannot be ruled out [65].

Concerning  $\text{Au}_x\text{Pd}_y$  alloy formation on ASA, two effects can arise; the so-called “ligand” effect, which evokes electronic interactions between electronically dissimilar components and the “geometric” effect, representing by the variation in composition, configuration and availability of active sites for a given reaction. For AuPtPd/ASA catalyst, the “geometric effect” can be inferred from the large enhancement of Pt and Pd surface exposure induced by the presence of gold particles (Table 3). However, the electron-deficiency of metal particles, which alters the metal-adsorbate bond strength, was excluded from XPS technique. This is because the electronic properties of the large metal crystallites are expected to be similar to those of bulk metal [65]. The absence of electronic modification could be beneficial for aromatics HYD since the self-inhibition of this reaction may be avoided [23]. In the case of electronic modification of noble metals, the aromatic hydrocarbons, which serve as electron donors, are more strongly adsorbed on electron-deficient active sites. As a consequence, the hydrogen dissociation on such sites is inhibited and self-inhibition of the hydrogenation activity occurs [52].

The lower initial activity of PtPd/MWNT than PtPd/ASA catalyst is expected considering that the latter catalyst has a larger BET specific area, acidity, and metal surface exposure. Moreover, the PtPd/MWNT sample is unique as it shows  $\text{Pd}^{2+}$  and  $\text{Pt}^{2+}$  ions in the close vicinity of chloride anions. From catalyst characterization, the morphology of PtPd/MWNT catalyst after reduction can be envisaged as large  $\text{Pd}^0$  and  $\text{Pt}_{48}\text{Pd}_{52}$  alloy aggregates and small  $\text{Pt}^0$  ( $d < 4$  nm) particles. Contrary to this sample, the PtPd/ASA catalyst possesses isolated  $\text{Pt}^0$  and  $\text{Pd}^0$  particles with no PtPd alloy formation. Contrary to platinum, Pd/C(Si) atomic ratios of both binary catalysts are much higher than of their respective bulk values. Thus, the main surface exposure of palladium on MWNT and ASA surfaces may be deduced. Taking these characteristics into account, possible explanations for the similar activity of PtPd on MWNT and ASA at TOS = 5 h might involve the ensemble effect of  $\text{Pt}_{48}\text{Pd}_{52}$  alloy formation on PtPd/MWNT and its relatively low deactivation during on-stream reaction (Table 4). The lowest  $E_a$  of the PtPd/MWNT catalyst could be explained in terms of the well known capacity of the MWNT for  $\text{H}_2$  storage [66] and assuming heterolytic dissociation of hydrogen on the surface Pt/Pd atoms of this catalyst. Moreover, in view of the large amount of impurities in the MWNT material, their influence on catalytic activity cannot be excluded [67].

Considering the strong affinity of gold for S-compounds [11], the observed S-resistance of the AuPtPd/ASA catalyst in aromatics HYD in the presence of DBT could be linked with the presence of  $\text{Au}_x\text{Pd}_y$  alloys and  $\text{Au}^0$  particles on its surface. This is consistent with a study of Canton et al. [19] who observed that in Au–Pd/C catalyst tested in benzaldehyde hydrogenation the formation of sulfide phase was delayed by the presence of gold. Since Au/SiO<sub>2</sub> catalyst was found to be active in DBT HDS at high  $\text{H}_2$  pressure (3.0 MPa) [16], the total DBT conversion in reaction of aromatics HYD at 523, 548 and 573 K is because at the high  $\text{H}_2$  pressure employed (2.0 MPa) the S-atom of the DBT molecule strongly binds to the gold atoms, and then the C–S bond is easily broken with subsequent formation of  $\text{H}_2\text{S}$ .

Contrary to AuPtPd/ASA, the strong deactivation of PtPd/MWNT in the reaction of benzene HYD in the presence of S was observed. The possible explanation of its deactivation involves S-poisoning deduced from the loss of metallic character of Pd, as confirmed by XPS (see Table 5). Knowing the electron acceptor character of the sulfur atom [68], the loss of metallic character of Pd suggests a modification of the original electronic properties of palladium particles when the catalyst comes into contact with sulfur. Taking into account the key role of acid sites in the S-tolerance of Pt and Pd particles when supported on highly acidic supports [7,69,70] as well as XPS data of used PtPd/MWNT (Fig. 10), it is more likely that accelerated deactivation of the PtPd/MWNT catalyst by S-compounds comes from benzene adsorption on acid sites. For this catalyst, the negative effect of low acidity on its S-resistance is not counterbalanced by PtPd alloy formation. Considering the work by Thomas et al. [71], this is probably because the S-resistance of PtPd alloys depends on the sulfur coverage: at low sulfur coverage reactivity is dominated by alloy formation whereas at high-sulfur coverage acidity plays a major role. The poor S-tolerance of PtPd/MWNT at low S-coverage was confirmed in a previous work [33].

In summary, it can be concluded that formation of  $\text{Au}_x\text{Pd}_y$  alloy, optimized surface acidity and increase of Pt/Pd surface exposure in the presence of  $\text{Au}^0$  species positively affect activity and thio-resistance of the AuPtPd/ASA catalyst. It is proposed that the presence of surface gold weakens the adsorption of aromatic compounds, thus facilitating product desorption.

#### 4. Conclusions

The addition of gold to the PtPd formulation as well as the use of amorphous silica–alumina as a support was found to be beneficial for the hydrogenation of aromatics in the absence and presence of S-compounds. The enhanced HYD activity observed with the ternary AuPtPd/ASA catalyst is related to its largest metal surface exposure and optimized acidity which allows the lowest catalyst deactivation during on-stream operation. The S-tolerance of AuPtPd/ASA catalyst was confirmed in simultaneous toluene and naphthalene hydrogenation in the presence of dibenzothiophene (100 ppm of S) and it was explained considering the “ensemble” effect of the alloy  $\text{Au}_x\text{Pd}_y$  formation, the presence of  $\text{Au}^0$  particles on the catalyst surface which enhance Pt/Pd species surface exposure as well as the moderate acidity of this sample. It is proposed that the presence of surface gold weakens the adsorption of aromatic compounds, thus facilitating product desorption. The easy S-poisoning of Pt–Pd when supported on MWNT in benzene HYD in the presence of 1-butanethiol is linked with the lowest acidity of this sample among the catalysts studied.

#### Acknowledgements

We thank Dr. M. Peña for TGA measurements. The Spanish Ministry of Science and Technology is also acknowledged for funding the PPQ2002-11841-E project.

## References

- [1] Official Journal of the European Union March 22, 2003 L 76/17.
- [2] G.B. McVicker, M. Daage, M.S. Touvelle, C.W. Hudson, D.P. Klein, W.C. Baird Jr., B.R. Cook, J.G. Chen, S. Hantzer, D.E.W. Vaughan, E.S. Ellis, O.C. Feeley, *J. Catal.* 210 (2002) 137.
- [3] U. Nylén, L. Sassu, S. Melis, S. Järås, M. Boutonnet, *Appl. Catal. A: Gen.* 299 (2006) 1.
- [4] U. Nylén, B. Pawelec, M. Boutonnet, J.L.G. Fierro, *Appl. Catal. A: Gen.* 299 (2006) 14.
- [5] B.H. Cooper, B.B.L. Donnis, *Appl. Catal. A: Gen.* 137 (1996) 203.
- [6] A. Stanislaus, B.H. Cooper, *Catal. Rev.-Sci. Eng.* 36 (1) (1994) 75.
- [7] R.M. Navarro, B. Pawelec, J.M. Trejo, R. Mariscal, J.L.G. Fierro, *J. Catal.* 189 (2000) 184.
- [8] H. Yasuda, T. Sato, Y. Yoshimura, *Catal. Today* 50 (1999) 6.
- [9] N. Matsubayashi, H. Yasuda, M. Imamura, Y. Yoshimura, *Catal. Today* 45 (1998) 375.
- [10] D.T. Thomson, *Platinum Met. Rev.* 48 (4) (2004) 169.
- [11] G.C. Bond, D.T. Thompson, *Catal. Rev. Sci. Eng.* 41 (3/4) (1999) 319.
- [12] R. Zanella, C. Louis, S. Giorgio, R. Touroude, *J. Catal.* 223 (2004) 328.
- [13] B.D. Chandler, A.B. Schabel, C.F. Blanford, L.H. Pignolet, *J. Catal.* 187 (1999) 367.
- [14] A.M. Venezia, V. La Parola, B. Pawelec, J.L.G. Fierro, *Appl. Catal. A: Gen.* 264 (1) (2004) 43.
- [15] B. Pawelec, A.M. Venezia, V. La Parola, E. Cano-Serrano, J.M. Campos-Martin, J.L.G. Fierro, *Appl. Surf. Sci.* 242 (2005) 380.
- [16] A.M. Venezia, V. La Parola, G. Deganello, B. Pawelec, J.L.G. Fierro, *J. Catal.* 215 (2003) 317.
- [17] A.M. Venezia, V. La Parola, V. Nicolí, G. Deganello, *J. Catal.* 212 (2002) 56.
- [18] B. Pawelec, E. Cano-Serrano, J.M. Campos-Martin, R.M. Navarro, S. Thomas, J.L.G. Fierro, *Appl. Catal. A: Gen.* 275 (1) (2004) 127.
- [19] P. Canton, M. Ferroni, C. Meneghini, F. Pinna, F. Menegazzo, N. Pernicone, A. Benedetti, *Proceedings of the 13th ICC, Paris, July, 2004, 01-052.*
- [20] W.M.H. Schatler, A.Yu. Stakheev, *Catal. Today* 12 (1992) 283.
- [21] S.T. Homeyer, W.M.H. Schatler, *Stud. Surf. Sci. Catal.* 49 (1989) 975.
- [22] S. Albertazzi, G. Busca, E. Finocchio, R. Glöckler, A. Vaccari, *J. Catal.* 223 (2004) 372.
- [23] E. Guillon, J. Lynch, D. Uzio, B. Didillon, *Catal. Today* 65 (2–4) (2001) 201.
- [24] S. Albertazzi, I. Baraldini, G. Busca, E. Finocchio, M. Lenarda, L. Storaro, A. Talon, A. Vaccari, *Appl. Clay Sci.* 29 (3/4) (2005) 224.
- [25] V. Lordi, N. Yao, *J. Mater. Res.* 15 (2000) 2770.
- [26] J.M. Planeix, N. Coustel, B. Coq, V. Brotons, P.S. Kumbhar, R. Dutartre, P. Geneste, P. Bernier, P.M. Ajayan, *J. Am. Chem. Soc.* 116 (1994) 7935.
- [27] A. Chambers, T. Nemes, N.M. Rodriguez, R.T.K. Baker, *J. Phys. Chem. B* 102 (1998) 2251.
- [28] H.P. Boehm, *Carbon* 32 (5) (1994) 759.
- [29] S.S. Barton, M.J.B. Evans, E. Halliop, J.A.F. MacDonald, *Carbon* 35 (1997) 1361.
- [30] C.N.R. Rao, A. Govindaraj, B.C. Satishkumar, *Chem. Commun.* (1996) 1525.
- [31] K. Niesz, A. Siska, I. Vesselényi, K. Hernadi, D. Méhn, G. Galbács, Z. Kónya, I. Kiricsi, *Catal. Today* 76 (1) (2002) 3.
- [32] J.M. Nhut, L. Pesant, J.P. Tessonnier, G. Winé, J. Guille, C. Pham-Huu, M.J. Ledoux, *Appl. Catal. A: Gen.* 254 (2003) 345.
- [33] B. Pawelec, V. La Parola, R.M. Navarro, S. Murcia-Marscarós, J.L.G. Fierro, *Carbon* 44 (1) (2006) 84.
- [34] N. Tushima, M. Harada, Y. Yamazaki, K. Asakura, *J. Phys. Chem.* 96 (1992) 9927.
- [35] H.P. Klug, *X-ray Diffraction Procedures for Polycrystalline and Amorphous Materials*, Wiley, New York, 1954.
- [36] A.R. West, *Solid State Chemistry and its Applications*, John Wiley and Sons Ltd., Chichester, England, 1998.
- [37] B. Pawelec, A.M. Venezia, V. La Parola, S. Thomas, J.L.G. Fierro, *Appl. Catal. A: Gen.* 283 (2005) 165.
- [38] D.A. Shirley, *Phys. Rev. B* 5 (1972) 4709.
- [39] P.M.A. Sherwood, in: D. Briggs, M.P. Seah (Eds.), *Practical Surface Analysis*, Wiley, New York, 1990, p. 181.
- [40] C.N. Satterfield, *Heterogeneous Catalysis in Industrial Practice*, 2nd ed., McGraw-Hill, 1980.
- [41] S.J. Gregg, K.S.W. Sing (Eds.), *Adsorption, Surface Area and Porosity*, 2nd ed., Academic Press, London, 1982.
- [42] T. Fujikawa, K. Idei, T. Ebihara, H. Mizuguchi, K. Usui, *Appl. Catal. A: Gen.* 192 (2) (2000) 253.
- [43] C. Mihut, C. Descorme, D. Duprez, M.D. Amiridis, *J. Catal.* 212 (2002) 125.
- [44] G. Pacchioni, S.-C. Chung, S. Krüger, N. Rösch, *Surf. Sci.* 392 (1997) 173.
- [45] H. Orita, N. Itoh, Y. Inada, *Surf. Sci.* 571 (2004) 161.
- [46] M. Wallin, H. Grönbeck, A. Lloyd Spetz, M. Skoglundh, *Appl. Surf. Sci.* 235 (2004) 87.
- [47] NIST Standard Reference Database Number 69, <http://webbook.nist.gov/chemistry/>.
- [48] C.M. Grill, R.D. Gonzalez, *J. Catal.* 64 (1980) 487.
- [49] E.L. Kugler, M. Boudart, *J. Catal.* 59 (1979) 201.
- [50] A.W. Weitkamp, *Adv. Catal.* 18 (1968) 1.
- [51] S. Jongpatiwut, Z. Li, D.E. Resasco, W.E. Alvarez, E.L. Sughrie, G.W. Dodwell, *Appl. Catal. A: Gen.* 262 (2) (2004) 241.
- [52] K. Ito, Y. Kogasaka, H. Kurokawa, M. Ohshima, K. Sugiyama, H. Miura, *Fuel Process. Technol.* 79 (2002) 77.
- [53] J. Shabtai, N.K. Nag, F.E. Massoth, in: M.J. Phillips, M. Ternan (Eds.), *Proceedings of the 9th International Congress on Catalysis, Calgary, 1988, vol. 1, Chem. Institute of Canada, Ottawa, 1988, p. 1.*
- [54] A. Sárkány, A. Horváth, A. Beck, *Appl. Catal. A: Gen.* 229 (2002) 117.
- [55] G. Neri, A.M. Visco, A. Donato, C. Milone, M. Malentacchi, G. Gubitosa, *Appl. Catal. A: Gen.* 110 (1994) 49.
- [56] N. Mahata, V. Vishwanathan, *J. Catal.* 196 (2000) 262.
- [57] C.D. Wagner, W.M. Riggs, L.E. Davis, J.F. Moulder, G.E. Muilenberg, *Handbook of X-ray Photoelectron Spectroscopy*, Perkin-Elmer Co., 1979.
- [58] T.H. Fleisch, R.F. Hicks, A.T. Bell, *J. Catal.* 87 (1984) 398.
- [59] C. Moreau, P. Geneste, in: J.B. Moffat (Ed.), *Theoretical Aspects of Heterogeneous Catalysis*, Van Nostrand Reinhold, New York, 1990, p. 256.
- [60] M.J. Sprague, J. Zheng, C. Song, *Am. Chem. Soc.* 47 (2) (2002) 103.
- [61] R.M. Navarro, B. Pawelec, P.T. Vasudevan, J.F. Cambra, P.L. Arias, *Fuel Process. Technol.* 61 (1999) 73.
- [62] T. Grzybek, K. Kreiner, *Langmuir* 13 (1997) 909.
- [63] Y. Xu, H. Shang, C. Liu, *Prep. Pap.-Am. Chem. Soc., Div. Pet. Chem.* 49 (1) (2004) 13.
- [64] A.F. Lee, C.J. Baddeley, C. Hardacre, R.M. Ormerod, R.M. Lambert, *J. Phys. Chem.* 99 (1995) 6096.
- [65] D. Poondi, M.A. Vannice, *J. Catal.* 161 (1996) 742.
- [66] M.T. Martínez, M.A. Callejas, A.M. Benito, M. Cochet, T. Seeger, A. Ansón, J. Schreiber, C. Gordon, C. Marhic, O. Chauvet, J.L.G. Fierro, W.K. Maser, *Carbon* 41 (2) (2003) 2247.
- [67] A. Lueking, R.T. Yang, *J. Catal.* 206 (2002) 165.
- [68] J.K. Lee, H.K. Rhee, *J. Catal.* 177 (1998) 208.
- [69] H. Yasuda, Y. Yoshimura, *Catal. Lett.* 46 (1997) 43.
- [70] H. Yasuda, N. Matsubayashi, T. Sato, Y. Yoshimura, *Catal. Lett.* 54 (1998) 23.
- [71] K. Thomas, C. Binet, T. Chevreau, D. Cornet, J.-P. Gilson, *J. Catal.* 212 (2002) 63.